

Towards Synchronism Through Dynamic Tides in J0651: the “Antiresonance” Locking

F. Valsecchi¹, W. M. Farr¹, B. Willems¹, and V. Kalogera¹

*Center for Interdisciplinary Exploration and Research in Astrophysics (CIERA) and
Department of Physics and Astronomy, Northwestern University, 2145 Sheridan Road,
Evanston, IL 60208, USA.*

francesca@u.northwestern.edu

ABSTRACT

In recent years, the Extremely Low Mass White Dwarf (ELM WD) survey has quintupled the number of known close, detached double WD binaries (DWD). The tightest such DWD, SDSS J065133.33+284423.3 (J0651), harbors a He WD eclipsing a C/O WD every $\simeq 12$ min. The orbital decay of this source was recently measured to be consistent with general relativistic (GR) radiation. Here we investigate the role of dynamic tides in a J0651-Like binary and we uncover the potentially new phenomenon of “antiresonance” locking. In the most probable scenario of an asynchronous binary at birth, we find that dynamic tides play a key role in explaining the measured GR-driven orbital decay, as they lock the system at stable antiresonances with the star’s eigenfrequencies. We show how such locking is naturally achieved and how, while locked at an antiresonance, GR drives the evolution of the orbital separation, while dynamic tides act to synchronize the spin of the He WD with the companion’s orbital motion, but *only on the GR timescale*. Given the relevant orbital and spin evolution timescales, the system is clearly on its way to synchronism, if not already synchronized.

Subject headings: binaries: eclipsing — binaries: general — stars: interiors — stars: oscillations — white dwarfs — gravitational waves

1. Introduction

Short period DWDs are the most numerous sources for the next generation of low-frequency (mHz) space-based gravitational wave (GW) detectors (e.g. LISA, Danzmann & the LISA study 1996, Hughes 2006, and eLISA/NGO, Amaro-Seoane et al. 2012). The eclipsing DWD SDSS

J065133.33+284423.3 (hereafter J0651, Brown et al. 2011; Hermes et al. 2012), discovered by the ELM WD survey (Brown et al. 2010, 2012; Kilic et al. 2010, 2011), harbors a tidally deformed He WD orbiting a C/O WD every $\simeq 12$ min; this is the shortest-period detached system known. Here, we investigate the effects of dynamic tides on the orbital evolution of this binary.

Previous investigations of tides in J0651 placed limit on the components’ tidal parameter Q , assuming tidal heating to be the cause of the observed luminosity (Piro 2011), or used polytropes to estimate the deviation from the pure GR-driven inspiral, under the assumption that the components are synchronized (Benacquista 2011).

The orbital evolution of detached DWDs is often assumed to be driven by GR emission alone. Willems et al. (2010) validated this assumption provided that the binary is in the regime of dissipative quasi-static tides (in the limit of orbital and rotational periods $\gg \sqrt{R^3(GM)^{-1}}$). The inefficiency of quasi-static tides means GR emission eventually drives the system out of synchronism and DWDs enter a regime in which dynamic tides and resonantly excited gravity modes (g -modes) must be taken into account.

Here, we use our newly developed tidally excited stellar pulsation code *CAFein* (Valsecchi et al. to be submitted) and detailed models of a J0651-Like He WD to study in detail the effect of radiative dissipation of dynamic tides on the orbital evolution of J0651. Our focus on radiative dissipation follows our understanding of dissipative dynamic tides in non-degenerate stars with radiative envelopes (Zahn 1975; Witte & Savonije 2001).

Fuller & Lai (2011, 2012) investigated the impact of *resonantly* excited g -modes on the orbital evolution of C/O DWDs. Dissipation in Fuller & Lai (2012) was treated via the so-called outgoing wave boundary condition (BC), which implicitly assumes that tides are efficiently damped via radiative damping or non-linear effects. The authors focused on the evolution of g -mode amplitudes *during* resonance, without a detailed treatment of tidal dissipation in and *out* of resonance, and found that resonant mode excitation could quickly drive the binary to (near) synchronization of the spin and orbit on the dynamic-tides timescale. Here, we reach fundamentally different conclusions: we find that, for a broad range of initial spin frequencies, dynamic tides act to drive the spin-orbit frequency mismatch to and trap it in an *antiresonance*, where the dissipation due to tides effectively vanishes. The orbit subsequently evolves due to GR emission, and the only action of tides is to keep the spin-orbit frequency difference trapped at the antiresonance value; as GR emission proceeds, both the spin and orbital frequencies increase, while their difference is locked, and the system is driven to synchronism, but this process takes place on the GR timescale.

Very recently, Hermes et al. (2012) reported the detection of orbital decay in J0651 consistent with the GR prediction. Here we show that dynamic tides potentially play a key role in such measurement, as they naturally drive the system into *antiresonance locking*, a new phenomenon we identify, with further evolution of the orbit occurring only on the GR timescale.

2. Observed and Model’s Properties

The DWD system J0651 was originally discovered by Brown et al. (2011). Hermes et al. (2012) measured an effective temperature, gravity, radius, and mass for the He WD of $T_{\text{eff}} = 16530 \pm 200 \text{ K}$, $\log(g) = 6.76 \pm 0.04 \text{ dex}$, $R_1 = 0.0371 \pm 0.0012 R_{\odot}$, and $M_1 = 0.26 \pm 0.04 M_{\odot}$; they also measured the C/O WD mass to be $0.5 \pm 0.04 M_{\odot}$ and the orbit is circular. The measured orbital period and orbital decay are $P = 765.206543(55) \text{ s}$ and $\dot{P} = (-9.8 \pm 2.8) \times 10^{-12} \text{ s s}^{-1}$, respectively. For comparison, the orbital period decay expected from GR emission alone is $\dot{P} = (-8.2 \pm 1.7) \times 10^{-12} \text{ s s}^{-1}$ for the masses derived by Hermes et al. (2012). We use MESA (Paxton et al. 2011) to create a He WD model with $T_{\text{eff}} \simeq 16766 \text{ K}$, $\log(g) = 6.68 \text{ dex}$, $R_1 = 0.0363 R_{\odot}$, and $M_1 = 0.23 M_{\odot}$. These parameters are within 1σ of the measured M_1 and R_1 and 2σ of the measured T_{eff} and $\log(g)$.

3. Tidal Evolution

3.1. Non-Adiabatic Stellar and Tidal Pulsations

When tides are dynamic, the tidal forcing exerted by a star in a binary can interact with one or more of the companion’s eigenfrequencies. Here we take the He WD (primary) to rotate uniformly with an angular velocity Ω_1 and, given the MESA model’s current cooling timescale t_{cool} (see below), we assume that its stellar parameters do not evolve. We also neglect the effects of Coriolis and centrifugal forces (the break-up spin for the model is $\simeq 2.5 \text{ min}$). Under these assumptions, the star’s eigenmodes correspond to those of a non-rotating spherically symmetric star in hydrostatic equilibrium. We treat the C/O WD (secondary) as a point mass. Let $\mathbf{r} = (r, \theta, \phi)$ be a system of spherical coordinates with respect to an orthogonal frame co-rotating with the primary. The system of equations governing non-adiabatic and non-radial stellar pulsations has been derived e.g. by Unno et al. (1989) (Eqs. 24.7 - 24.12 in §24). It comprises six homogeneous ordinary differential equations involving the complex dimensionless eigenfrequency ω ($\sigma = \omega \sqrt{GM/R^3}$, where σ is

the dimensional eigenfrequency). It is convenient to use

$$\begin{aligned} y_1 &= \frac{\xi_r}{r}, \quad y_2 = \frac{1}{gr} \left(\frac{p'}{\rho} + \Phi' \right) = \frac{\omega^2 r}{g} \frac{\xi_h}{r}, \quad y_3 = \frac{1}{gr} \Phi' \\ y_4 &= \frac{1}{g} \frac{d\Phi'}{dr}, \quad y_5 = \frac{\delta S}{c_p}, \quad y_6 = \frac{\delta L_R}{L_R} \end{aligned} \quad (1)$$

as integration variables in the eigenvalue problem. Here ξ_r and ξ_h are the radial and orthogonal component of the displacement of the star's mass element from the equilibrium position, ρ the density, c_p the specific heat at constant pressure, and p' , Φ' , δS , and δL_R the perturbed pressure, potential of self-gravity, entropy and radiative luminosity, respectively. The effect of convection on the oscillations is neglected.

The central BCs are that the entropy is constant during a single oscillation ($\delta S = 0$) and that Φ' , $(p'/\rho + \Phi')$, and ξ_r are regular. The surface BCs are determined by assuming that near the surface the pressure and the density drop steeply outward, by considering that there is no inward radiative flux, and by requiring the continuity of Φ' and its first derivative.

The tidal action from the companion is included as a small time-dependent force which perturbs the hydrostatic equilibrium of a spherically symmetric static star. The system of equations describing the tidal response of the star is formally identical to the equations describing pure stellar pulsations, provided that the perturbed potential of self-gravity Φ' is replaced by the total perturbation of the potential $\Psi = \Phi' + \epsilon_T W$, where $\epsilon_T W$ is the tide-generating potential. We expand $\epsilon_T W$ in a Fourier series as (see e.g. Polfiet & Smeyers 1990)

$$\epsilon_T W(\mathbf{r}, t) = -\epsilon_T \sum_{l=2}^4 \sum_{m=-l}^l \sum_{k=-\infty}^{\infty} c_{l,m,k} \left(\frac{r}{R_1} \right)^l Y_l^m(\theta, \phi) \exp[i(\sigma_{m,k} t - k\Omega_{\text{orb}} \tau)] \quad (2)$$

where $Y_l^m(\theta, \phi)$ are unnormalized spherical harmonics of harmonic degree l , and azimuthal number m , and k is the Fourier index; θ is the colatitude in the WD's co-rotating frame, and ϕ is the longitude. At time $t = 0$, the angle $\phi = 0$ marks the position of the periastron. The dimensionless parameter $\epsilon_T \equiv (R_1/a)^3 (M_2/M_1)$ gives the ratio of the tidal force to gravity at the star's equator. The semi-major axis of the binary is a , Ω_{orb} is the mean motion, τ the time at periastron passage, $\sigma_{m,k} = k\Omega_{\text{orb}} + m\Omega_1$ is the tidal forcing angular frequency with respect to the co-rotating frame, and $c_{l,m,k}$ are Fourier coefficients. For a binary with a circular orbit (like J0651) the only non-zero $c_{l,m,k}$ are the ones with $k = -m$ and are defined as

$$c_{l,m,-m} = \frac{(l - |m|)!}{(l + |m|)!} P_l^{|m|}(0) \left(\frac{R_1}{a} \right)^{l-2} \quad (3)$$

where $P_l^m(x)$ are Legendre polynomials of the first kind. Refer to Polfiet & Smeyers (1990) for further discussion of $c_{l,m,k}$. The expansion (2) shows that the tidal action from the secondary induces in the primary an infinite number of forcing angular frequencies $\sigma_{m,k}$. Tides are dynamic when $\sigma_{m,k} \neq 0$.

In principle, all values of l , m , and k must be considered in the set of equations describing tidally excited stellar pulsations. However, as $c_{l,m,k} \propto (R_1/a)^{l-2}$, investigations on dynamic tides are often restricted to the terms belonging to $l = 2$. Here we consider only the leading term in the expansion of $\epsilon_T W$: $(l, m, k) = (2, -2, 2)$.

3.2. Secular Evolution of the Orbital Separation and Stellar Spin

Here we summarize the main equations describing the secular evolution of a and Ω_1 due to dynamic tides for a binary with a circular orbit and for $(l, m, k) = (2, -2, 2)$; refer to Willems et al. (2003, 2010) for a more detailed derivation and for an explanation of the various parameters entering such equations.

The primary's tidal deformation perturbs the external gravitational field, and thus the Keplerian motion of the binary components. In the framework of the theory of osculating elements in celestial mechanics (Sterne 1960; Brouwer & Clemence 1961; Fitzpatrick 1970), the rate of change of the orbital semi-major axis due to the tidal deformation of the star is given by

$$\left(\frac{da}{dt}\right)_{\text{sec}} = \frac{8\pi}{P_{\text{orb}}} \frac{M_2}{M_1} a \left(\frac{R_1}{a}\right)^{l+3} |F_{l,m,k}| \sin \gamma_{l,m,k} G_{l,m,k}^{(2)}(0) \quad (4)$$

where $G_{l,m,-m}^{(2)}(0) = -2mP_l^{|m|}(0)c_{l,m,-m}$ for $e = 0$, P_{orb} is the orbital period, and the dimensionless $F_{l,m,k}$ are defined as

$$F_{l,m,k} = -\frac{1}{2} \left[\frac{R_1}{GM_1} \frac{\Psi_{l,m,k}(R_1)}{\epsilon_T c_{l,m,k}} + 1 \right] = |F_{l,m,k}| e^{i\gamma_{l,m,k}} \quad (5)$$

and measure the response of the star to the various tidal forcing frequencies; $F_{l,m,k}$ can be computed from a solution to the modified pulsation equations described above. The angle $\gamma_{l,m,k}$ describes the phase-lag between the tidal forcing and the response of the total potential induced by the dissipation in the system.

This phase shift produces a torque on the tidally deformed star, which acts on its spin yielding

$$\left(\frac{d\Omega_1}{dt}\right)_{\text{sec}} = -\frac{8\pi}{P_{\text{orb}}} \left(\frac{GM_1^2 M_2^2}{M_1 + M_2}\right)^{1/2} \frac{M_2}{M_1} \frac{a^{1/2}}{I_1} \left(\frac{R_1}{a}\right)^{l+3} |F_{l,m,k}| \sin \gamma_{l,m,k} \frac{G_{l,m,k}^{(2)}(0)}{2} \quad (6)$$

4. The Dynamic tides regime in a J0651-Like binary

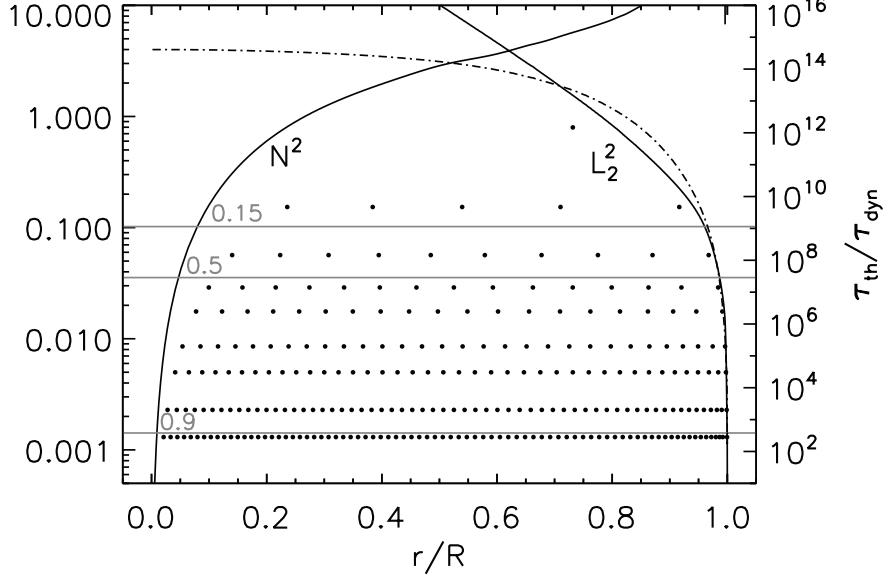


Fig. 1.— *Left y-axis:* radial profile of the Brünt-Vaisala (N) and Lamb (L_2) frequencies squared (black-solid lines). The dots mark the positions of the nodes for the modes $g_1, g_5, g_{10}, g_{15}, g_{20}, g_{30}, g_{40}, g_{60}, g_{80}$. The horizontal grey lines mark the position of the tidal forcing frequencies ω_T^2 for spins (from top to bottom) $\Omega_1 = 0.15 \Omega_{\text{orb}}$, $\Omega_1 = 0.5 \Omega_{\text{orb}}$, and $\Omega_1 = 0.9 \Omega_{\text{orb}}$. All the frequencies are normalized by $\sqrt{GM/R^3}$. *Right y-axis:* the dashed-dot line shows the ratio of the star’s thermal to dynamical ($\tau_{\text{dyn}}/\tau_{\text{th}}$) timescales. Where $\tau_{\text{dyn}}/\tau_{\text{th}}$ is small non-adiabaticity becomes relevant.

Here we first examine whether dynamic tides are relevant in a J0651-Like binary by comparing the He WD eigenfrequencies with the tidal forcing frequencies. We use *CAFein* (Valsecchi et al. to be submitted) to compute the non-adiabatic $l = 2$ eigenfrequencies for g – modes between g_1 – g_{80} . The complex eigenfrequencies are summarized in Table 1. In Fig. 1 we show the propagation diagram for a J0651-Like He WD, where the squared Brünt-Vaisala frequency is $N^2 = g(\Gamma_1^{-1} d \ln \rho / dr - d \ln \rho / dr)$ (Brassard et al. 1991), while the squared Lamb frequency is given by $L_1^2 = l(l+1)c_s^2/r^2$. The g -modes propagate in regions where $\omega_R^2 < N^2$ and L_1^2 . The dots in Fig. 1 mark the positions of the radial nodes for the modes considered in Table 1, while the horizontal grey lines mark the position of the tidal forcing frequency (ω_T^2) if Ω_1 is varied. As ω_T^2 and ω_R^2 cover the same frequency regime, resonances between tides and eigenmodes can be relevant for a J0651-Like binary, and hence tides are dynamic in this system.

Table 1: Non-adiabatic eigenfrequencies for a J0651-Like He WD. The subscripts “R” and “I” denote the real and imaginary part, respectively. Note that $|\omega_I|$ increases with the order of the mode, indicating that non-adiabaticity becomes relevant for high-order modes (see Fig. 1). Also, $\omega_I < 0$ for modes up to g_{19} , indicating that these modes are unstable.

mode	ω_R	ω_I
g_1	$8.928 \cdot 10^{-1}$	$\simeq 10^{-14}$
g_5	$3.915 \cdot 10^{-1}$	$-1.65 \cdot 10^{-11}$
g_{10}	$2.379 \cdot 10^{-1}$	$-1.057 \cdot 10^{-9}$
g_{15}	$1.701 \cdot 10^{-1}$	$-7.804 \cdot 10^{-9}$
g_{20}	$1.326 \cdot 10^{-1}$	$8.403 \cdot 10^{-9}$
g_{30}	$9.237 \cdot 10^{-2}$	$1.959 \cdot 10^{-6}$
g_{40}	$7.065 \cdot 10^{-2}$	$9.882 \cdot 10^{-6}$
g_{60}	$4.785 \cdot 10^{-2}$	$2.842 \cdot 10^{-5}$
g_{80}	$3.611 \cdot 10^{-2}$	$5.519 \cdot 10^{-5}$

5. Synchronism Through Dynamic Tides : the Antiresonance Locking

In Fig. 2 we show the timescales for the evolution of a and Ω_1 due to tides calculated using Eqs. (4) and (6). We fix Ω_{orb} and M_2 to the currently observed values and vary Ω_1 , thus changing ω_T . Here we consider Ω_1 ranging between $\simeq (0.15-0.999) \Omega_{\text{orb}}$. Black and grey data points represent positive and negative timescales, respectively. As expected, $\dot{a}_{\text{sec}} < 0$ when $\dot{\Omega}_{1,\text{sec}} > 0$ and vice versa. Note that Ω_1 evolves faster than a by about 2 orders of magnitude. Dips in the timescales correspond to resonances between the tidal forcing frequencies and the star’s eigenfrequencies, while the peaks mark the “antiresonances”.

The sign of the timescales depends on the angle that parametrizes tidal dissipation, $\gamma_{l,m,k}$. This angle, in turn, is related to the physical angle ϕ describing the orientation of the bulge in the star’s reference frame via

$$\phi = -\gamma_{l,m,k}/m, \quad (7)$$

or for $m = -2$, $\phi = \gamma/2$.

When $\gamma_{2,-2,2} = 0$ or π , the rate of change of a and Ω_1 becomes zero and the timescales display an antiresonance. At these lag angles the bulge is either aligned with the companion or $\pi/2$ out of alignment; in either case there is no tidal torque and therefore no change in the orbit or spin due to tides. On the other hand, resonances occur when $\gamma_{2,-2,2}$ equals either $\pi/2$ or $-\pi/2$, and thus ϕ equal to $\pi/4$ or $-\pi/4$; in these configurations, the torque is at a

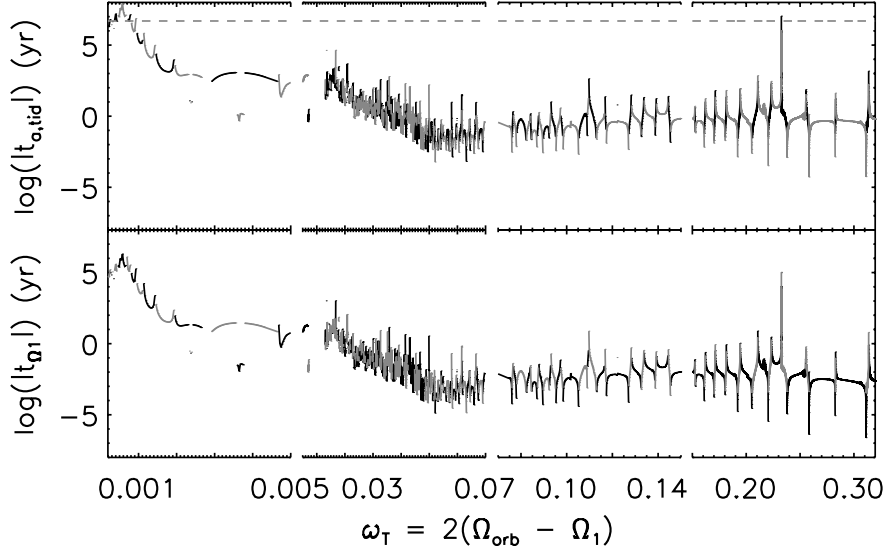


Fig. 2.— Timescales for the secular evolution of orbital separation and stellar spin due to dynamic tides. *Top*: $\log|t_{a,tid}| = \log|a/\dot{a}_{\text{sec}}|$. The horizontal dashed line shows the theoretically expected GR timescale $\log|t_{a,\text{GR}}|$ from Peters (1964) for the masses considered here ($t_{a,\text{GR}} \simeq 5 \text{ Myr}$). *Bottom*: $\log|t_{\Omega_1}| = \log|\Omega_1/\dot{\Omega}_{1,\text{sec}}|$. Grey and black lines and data points correspond to negative and positive timescales, respectively. As a reference, the first dip on the right marks the g_7 -mode resonance. Note that the x-axis is not uniform, and that $|t_{\Omega_1}| \simeq 10^{-2} |t_{a,tid}|$.

maximum.

The agreement between the observed orbital decay and the GR prediction implies that tides are not currently affecting the orbit. If the He WD were born close to synchronization or evolved to synchronism with the companion’s orbital motion, tides are quasi-static ($\omega_T \ll 1$) or static ($\omega_T = 0$) and the orbital evolution timescales due to quasi-static tides are longer than the theoretical GR timescale (see Fig. 2 or Willems et al. 2010). On the other hand, if the He WD were born in or evolved to an asynchronous state, the signs of the timescales in Fig. 2 can result in spin evolution that stably locks the star at antiresonances, where $t_{a,tid} > t_{a,\text{GR}}$ (see details below). The crossing of the antiresonance peaks with the horizontal dashed line in Fig. 2 is visible only for $\omega_T \simeq 0.23$ because of the resolution adopted during the scan of the parameter space in Ω_1 , but $t_{a,tid} \gg t_{a,\text{GR}}$ whenever the angle $\gamma_{l,m,k}$ in Eq. (4) passes through 0 and π .

Fig. 3 describes in detail the spin evolution that results in antiresonance locking. For a binary on the left of the leftmost peak in the figure, where $\dot{\Omega}_1 < 0$, dynamic tides act on Ω_1 and move the binary to the right eventually reaching the antiresonance. At antiresonance

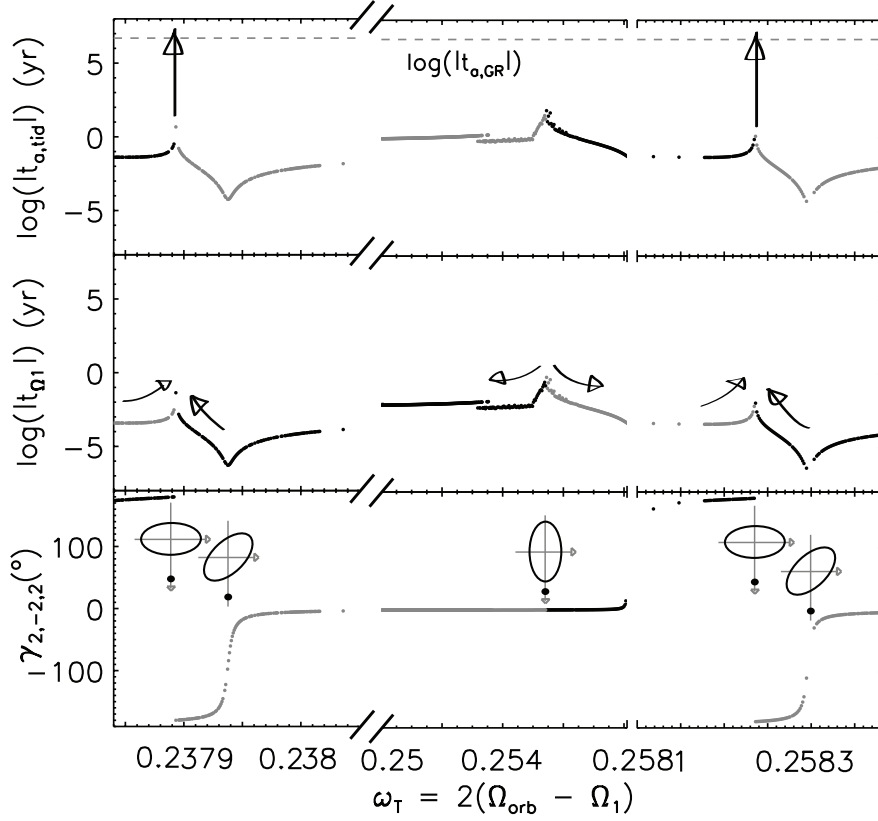


Fig. 3.— Resonances with the modes g_9 and g_{10} and antiresonance locking. The various symbols are as in Fig. 2 with the addition of $\gamma_{2,-2,2}$ and a cartoon depicting the orientation of the tidal bulges in the star’s frame (the black-filled circle denotes the companion). The arrows indicate the directions towards which dynamic tides drive a J0651-Like binary (see text); antiresonances where $\dot{\Omega}_1 < 0$ and $\dot{\Omega}_1 > 0$ on the left side and right side, respectively, are trapping. Once trapped, $\omega_T = 2(\Omega_{\text{orb}} - \Omega_1)$ is constant, while the subsequent GW emission implies $\dot{\Omega}_{\text{orb}} = \dot{\Omega}_1 > 0$, so that $\Omega_1/\Omega_{\text{orb}} \rightarrow 1$. Note that the x-axis in this figure is not uniform.

$t_{a,\text{tid}} > t_{a,\text{GR}}$ and GR drives orbital shrinkage without affecting Ω_1 . As Ω_{orb} increases and the binary moves to the right of the peak, dynamic tides act on the spin to bring it back at antiresonance. This stable antiresonance locking occurs for each antiresonance with $\dot{\Omega}_1 < 0$ and $\dot{\Omega}_1 > 0$ on the left side and right side, respectively. On the other hand, the antiresonance in the middle panel of Fig. 3 and all regular resonances are unstable, as dynamic tides quickly drive the binary out of them.

Mathematically, antiresonance locking is analogous to typical resonance locking (as discussed e.g., by Witte & Savonije 1999). If the star is locked at an antiresonance frequency

ω_α , then $\dot{\omega}_T = \dot{\omega}_\alpha$. Assuming the background model doesn’t evolve yields $\dot{\omega}_\alpha = 0$ and thus $\dot{\omega}_T = 0$. The latter assumption is justified here as for the MESA model $t_{\text{cool}} \simeq 90$ Myr and it is longer than the relevant timescales considered. As ω_T is constant, $\dot{\Omega}_{\text{orb}} = \dot{\Omega}_1$ and, since at antiresonance locking GR shrinks the orbit, $\dot{\Omega}_{\text{orb}} = \dot{\Omega}_1 > 0$. The latter implies that the combination of orbital shrinkage due to GR and of antiresonance locking due to dynamic tides brings the He WD to synchronization with the companion’s orbital motion on the GR timescale. In fact, defining $r = \Omega_1/\Omega_{\text{orb}}$, we find $\dot{r} \propto \dot{\Omega}_{\text{orb}}(\Omega_{\text{orb}} - \Omega_1) > 0$. Since the absolute difference between Ω_1 and Ω_{orb} is fixed by the antiresonance condition and both $|\Omega_1|$ and $|\Omega_{\text{orb}}|$ are increasing, $r \rightarrow 1$ on a timescale $t_r = r/\dot{r} = -(2/3)t_{\text{GR}}\Omega_1(\Omega_{\text{orb}} - \Omega_1)^{-1}$.

Consequently, the binary, while locked in antiresonance, it is driven to synchronism because of the GR-driven orbital decay. Whether J0561 has achieved synchronism already or it remains locked at antiresonance, still on its way to synchronism depends on the relative magnitude of the timescales involved (t_r , t_{GR} , and t_{cool}), as well as their history, linked to the initial properties of the system. Answering this question requires coupled time intergration for a range of initial conditions, an analysis that is beyond the scope of the present study focusing on the new phenomenon of antiresonance locking; such a study will be the subject of future work.

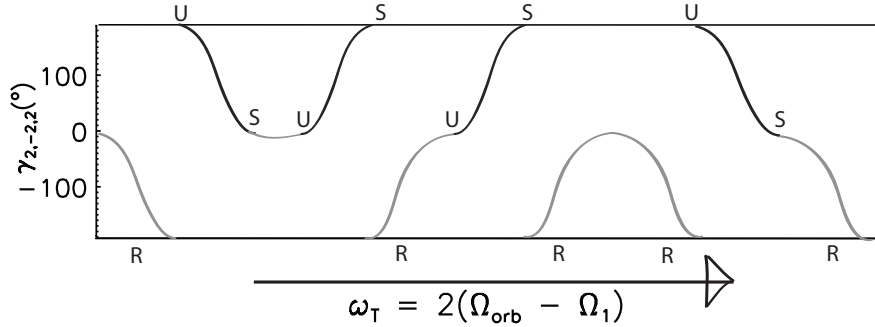


Fig. 4.— Possible combinations for $\gamma_{2,-2,2}$ in crossing two consecutive resonances (R), when the crossing occurs at $\gamma_{2,-2,2} = -\pi/2$. Black and grey lines denote positive and negative $\gamma_{2,-2,2}$, respectively. We use “S” and “U” to mark stable and unstable antiresonances.

Even though it is difficult to identify all the stable antiresonances in Fig. 2 at the shown resolution, the number of antiresonances expected between two resonances can be determined from the change in the angle $\gamma_{2,-2,2}$ in the passage through two consecutive resonances, as shown in Fig. 4. This illustration shows all possible combinations in $\gamma_{2,-2,2}$ when the resonance occurs at $\gamma_{2,-2,2} = -\pi/2$ (a similar picture can be drawn for resonances occurring at $\gamma_{2,-2,2} = \pi/2$). The number of antiresonances expected is either none, two, or four. For the latter two cases, we expect alternating stable and unstable antiresonances. The effect of resonances and unstable antiresonances is to drive the binary towards the

closest stable antiresonance. This behavior is generic for any object under the influence of non-adiabatic dynamic tides, if the evolution of its properties are neglected; the locations of the resonances and antiresonances depend on the details of the object’s structure, but the general picture of antiresonance locking depends only on the continuity of the phase $\gamma_{l,m,k}$ between resonances.

6. Conclusions

In this Letter, we show that dissipative dynamic tides potentially play a key role in explaining the recently measured orbital decay of J0651 (Hermes et al. 2012), even though their effects are not directly apparent. In fact, in the most probable scenario in which the binary was asynchronous at birth, the agreement between the observed orbital decay and the GR prediction is achieved through the new phenomenon of antiresonance locking identified here. Assuming the He WD doesn’t evolve on a relevant timescale, dynamic tides naturally lock the system at stable antiresonances with the star’s eigenfrequencies. While locked, GR drives the evolution of the orbital separation, with dynamic tides maintaining the antiresonance condition and drive the binary to synchronism *on the GR timescale*. Time integration of the binary orbit for a wide range of initial conditions and a self-consistent calculation of all the relevant timescales will allow to assess whether the system is still locked and away from synchronism or if it has had time to reach synchronism. Future measurements of the He WD spin can potentially provide a check of the theoretical predictions presented here.

We are grateful to C. Deloye, A. Barker, Y. Lithwick, M. Kilic, A. Gianninas, and W. Brown for useful discussions during the development of this project. Simulations were performed on the computing cluster **Fugu** available to the Theoretical Astrophysics group at Northwestern and partially funded by NSF grant PHY-0619274 to VK. This work was supported by NASA Award NNX09AJ56G to V.K.

REFERENCES

- Amaro-Seoane, P., et al. 2012, *Classical and Quantum Gravity*, 29, 124016
- Benacquista, M. J. 2011, *ApJ*, 740, L54+
- Brassard, P., Fontaine, G., Wesemael, F., Kawaler, S. D., & Tassoul, M. 1991, *ApJ*, 367, 601
- Brouwer, D., & Clemence, G. M. 1961, *Methods of celestial mechanics*
- Brown, W. R., Kilic, M., Allende Prieto, C., & Kenyon, S. J. 2010, *ApJ*, 723, 1072
- . 2012, *ApJ*, 744, 142
- Brown, W. R., Kilic, M., Hermes, J. J., Allende Prieto, C., Kenyon, S. J., & Winget, D. E. 2011, *ApJ*, 737, L23+
- Danzmann, K., & the LISA study team. 1996, *Classical and Quantum Gravity*, 13, 247
- Fitzpatrick, P. M. 1970, *Principles of celestial mechanics*
- Fuller, J., & Lai, D. 2011, *MNRAS*, 412, 1331
- . 2012, *MNRAS*, 421, 426
- Hermes, J. J., et al. 2012, *ApJ*, 757, L21
- Hughes, S. A. 2006, in *American Institute of Physics Conference Series*, Vol. 873, *Laser Interferometer Space Antenna: 6th International LISA Symposium*, ed. S. M. Merkowitz & J. C. Livas, 13–20
- Kilic, M., Brown, W. R., Allende Prieto, C., Agüeros, M. A., Heinke, C., & Kenyon, S. J. 2011, *ApJ*, 727, 3
- Kilic, M., Brown, W. R., Allende Prieto, C., Kenyon, S. J., & Panei, J. A. 2010, *ApJ*, 716, 122
- Paxton, B., Bildsten, L., Dotter, A., Herwig, F., Lesaffre, P., & Timmes, F. 2011, *ApJS*, 192, 3
- Peters, P. C. 1964, *Physical Review*, 136, 1224
- Piro, A. L. 2011, *ApJ*, 740, L53+
- Polfliet, R., & Smeyers, P. 1990, *A&A*, 237, 110

- Sterne, T. E. 1960, *An introduction to celestial mechanics*
- Unno, W., Osaki, Y., Ando, H., Saio, H., & Shibahashi, H. 1989, *Nonradial oscillations of stars*, ed. Unno, W., Osaki, Y., Ando, H., Saio, H., & Shibahashi, H.
- Willems, B., Deloye, C. J., & Kalogera, V. 2010, *ApJ*, 713, 239
- Willems, B., van Hoolst, T., & Smeyers, P. 2003, *A&A*, 397, 973
- Witte, M. G., & Savonije, G. J. 1999, *A&A*, 350, 129
- . 2001, *A&A*, 366, 840
- Zahn, J.-P. 1975, *A&A*, 41, 329